Journal of the Ceramic Society of Japan 130 [7] 452-457 2022
DOI http://doi.org/10.2109/jcersj2.21190

JCS-Japan

FULL PAPER

Lattice deformation and phase transition of aluminum nitride studied by density functional theory calculations

Kota Hasegawa[1,2], Takao Shimizu[2,3] and Naoki Ohashi[1,2,4,†]

[1] Interdisciplinary Graduate school of Engineering Sciences, Kyushu University, 6–1 Kasuga-koen, Kasuga, Fukuoka 816–8580, Japan
[2] National Institute for Materials Science, 1–1 Namiki, Tsukuba, Ibaraki 305–0044, Japan
[3] JST-PRESTO, Japan Science and Technology Agency, 4–1–8 Honcho, Kawaguchi, Saitama 332–0012, Japan
[4] Materials Research Center for Element Strategy (MCES), Tokyo Institute of Technology, 4259 Nagatsuta, Midori-ku, Yokohama 226–8503, Japan

The density functional theory (DFT) was employed to understand the ferroelectric behaviors of wurtzite (WZ)-type aluminum nitride (AlN). To explain the decrease in the coercive field (E_c) due to lattice deformation, the total energy and enthalpy of the strained WZ phase were compared to those of the non-polar (NP) phase, which acted as a transition state during polarity switching. The shrinkage of the *c*-axis length and elongation of the *a*-axis length were favorable for reducing E_c. In addition, the calculated residual stress in the transient NP phase was as high as 30 GPa, suggesting that such a high residual stress may be related to the polarity switching behavior under a very high electric field.

Key-words : Aluminum nitride, Ferroelectricity, Density functional theory, Lattice deformation

[Received December 31, 2021; Accepted March 14, 2022]

1. Introduction

Wurtzite-type (WZ-type) nitrides, that is, aluminum nitride (AlN), gallium nitride (GaN), indium nitride (InN), and their alloys, have been extensively developed as materials for optoelectronic devices.[1)] Furthermore, nitride semiconductors are used in switching devices for electric power management because they possess a very high dielectric strength due to their relatively wide electron energy bandgap.[2)] Consequently, most previous studies on WZ-type semiconductors have focused on charge carrier injection and carrier transport behaviors that provide the basis for efficient electronics with low energy consumption. On the other hand, these WZ-type nitrides are also attracting increased attention for their piezoelectricity, because they belong to the non-centrosymmetric $P6_3mc$ space group. For instance, WZ-type aluminum-scandium nitride [$(Al_{1-x}Sc_x)N$] has been used in electromechanical coupling devices.[3),4)] In particular, WZ-type $(Al_{1-x}Sc_x)N$ has been employed as a piezoelectric material in film bulk acoustic resonators for high-frequency filter applications in telecommunication technologies[5)] because of its relatively high piezoelectric performance. However, the spontaneous polarization of WZ-type nitrides has emerged as a critical issue not only for piezoelectric applications but also for electronic and optoelectronic applications, because the charge transport and distribution are significantly altered in these semiconductor devices due to polarization. Hence, many experimental and theoretical studies relating to the polarization and polar surfaces/interfaces of WZ-type compounds have been performed.[6)] In particular, the surface termination of epitaxial WZ-type semiconductor films, which can either be anion(X^{q-})-terminated or metal-cation(M^{q+})-terminated, is regarded as a key issue in the fabrication of electronic devices.

Here, it must also be noted that many metal nitrides, such as scandium nitride (ScN), possess cubic rather than polar symmetry, i.e., they exist in a rock-salt type structure. Consequently, a miscibility gap exists in some nitride alloy systems, such as the pseudo-binary system formed by WZ-type AlN and rock-salt-type ScN.[7)] With the aim of discovering high-performance piezoelectric materials in nitride systems, many studies have been conducted on $(Al_{1-x}Y_x)N$,[8)] $(Al_{1-x}B_x)N$,[8)] $(Al_{1-x}Yb_x)N$,[9)] $(Al_{1-x}Cr_x)N$,[10)] $(Al_{1-x}Ta_x)N$,[11)] $(Al_{1-x}Er_x)N$,[12)] $[Al_{1-x}(Mg_{1/2}Zr_{1/2})_x]N$,[13)] $[Al_{1-x}(Mg_{1/2}Hf_{1/2})_x]N$,[14)] $[Al_{1-x}(Mg_{2/3}Nb_{1/3})_x]N$,[15)] and $(Ga_{1-x}Sc_x)N$[16)] systems, focusing on the stability of the WZ form and piezoelectric performance.

Investigations on WZ-type compounds entered a new era when Fichtner et al.[17)] discovered that WZ-type (Al,Sc)N exhibited ferroelectricity. It was found that the

† Corresponding author: N. Ohashi; E-mail: ohashi.Naoki@nims.go.jp
‡ Preface for this article: DOI http://doi.org/10.2109/jcersj2.130.P7-1

N-terminated $(000\bar{1})$ surface transforms into the (Al,Sc)-terminated (0001) surface and vice versa through the application of a high electric field. Subsequently, a similar ferroelectric behavior was reported in other WZ-type compounds, including $(Al_{1-x}B_x)N$,[18),19)] $(Zn_{1-x}Mg_x)O$,[20)] $(Ga_{1-x}Sc_x)N$,[21),22)] and AlN.[19)] The ferroelectric properties of WZ-type $(Al_{1-x}Sc_x)N$ are characterized by an extremely high remnant polarization ($P_r = 80$–$120\,\mu C/cm^2$) and an unusually high coercive field ($E_c = 3$–$5\,MV/cm$).[17),23)] The E_c of $(Al_{1-x}Sc_x)N$ is one order of magnitude higher than those of $PbZr_{1-x}Ti_xO_3$ (PZT) and $BaTiO_3$, which is unfavorable for practical applications. The properties of WZ-type $(Al_{1-x}Sc_x)N$ strongly depend on its composition. It has been reported that increasing the Sc concentration (x) in $(Al_{1-x}Sc_x)N$ can decrease E_c but leads to a degradation in the dielectric properties, such as the breakdown voltage.[24)] Therefore, reducing E_c without degrading the dielectric properties is essential for the development of WZ-type ferroelectric materials with optimal properties.

The mechanism of ferroelectricity in WZ-type compounds at the atomic scale has been investigated mostly through theoretical calculations, particularly by the density functional theory (DFT).[25)–31)] The most likely polarization reversal motion in WZ-type compounds under an electric field is the movement of X^{q-} and M^{q+} in opposite directions along the c-axis. As shown in **Fig. 1**, the polar WZ-type structure [Figs. 1(a) and 1(c)] transforms to a non-polar (NP) structure with the $P6_3/mmc$ space group [Fig. 1(b)] as a transition state during polarization reversal.[25)–27)] Under this assumption, the transition state in Fig. 1(b) is the saddle point in the energy diagram for polarization reversal. Therefore, the enthalpy difference between the WZ and NP structures corresponds to the activation energy for the polarity change of the WZ-type lattice.

As noted by Moriwake et al., the M–X distance in the NP structure is a highly important parameter for the occurrence of polarization reversal.[27)] Yazawa et al. concluded from their experimental study that the E_c of ferroelectric $(Al_{1-x}Sc_x)N$ films is strongly correlated with their lattice parameters (c/a ratio).[32)] Hence, it is essential to correlate the lattice constants to the ferroelectricity in WZ-type structures. In experimental investigations, the most typical approach for changing lattice parameters is through elemental substitution, e.g., the substitution of Sc for Al in AlN. While such a substitution effectively modifies the lattice parameters, it also simultaneously changes the nature of the chemical bonding (e.g. covalency or ionicity) of the M–X bonds because of the different electronegativities and ionicities of Al and Sc. Therefore, the contributions of the lattice parameters and characteristics of the constituent elements to the ferroelectric behavior cannot be distinguished by experimental measurements.

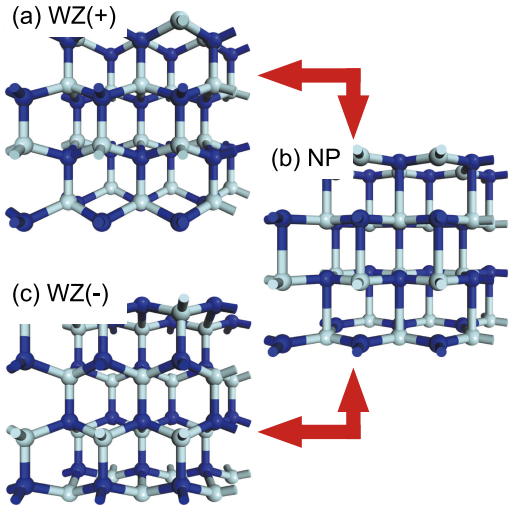

Fig. 1. Schematic of polarization reversal in a WZ-type crystal through a transient NP structure belonging to $P6_3/mmc$ symmetry.

In this context, visualization of the deformation behavior of WZ-type compounds is necessary to understand the ferroelectricity in WZ-type compounds. Therefore, in this study, DFT calculations were employed to investigate the structural features of AlN crystallized in the WZ phase with the $P6_3/mmc$ space group and the NP phase with the $P6_3/mmc$ space group. Briefly, we investigated a strongly strained pure AlN lattice in order to separate the effects of elemental substitution and lattice deformation. Riah et al.[33)] investigated the piezoelectricity and ferroelectricity of WZ-type nitrides in the form of heteroepitaxial thin films, and reported that the lattice mismatch between the substrate and film gives rise to a residual strain in the crystalline lattice. Their results suggested that the variations in the lattice parameters were induced by the lattice mismatch between the films and substrates. These findings support our idea that investigating the lattice deformation is crucial for understanding the piezoelectricity and ferroelectricity in WZ-type compounds. For this purpose, the total energies of the strained WZ and NP phases were calculated to explain the possible reduction in E_c in AlN.

2. Calculation method

The structural stability of AlN and the possible transformation from the WZ type to NP type were examined by DFT calculations carried out using the CASTEP simulation package.[34)] Conventional unit cells with two Al and two N atoms were employed as the model systems to study the effect of deformation. Norm-conserving pseudopotentials were used, and the Perdew-Burke-Ernzerhof generalized gradient approximation optimized for solids (abbreviated as PBEsol)[35)] was adopted as the exchange–correlation functional for self-consistent field (SCF) calculations. The cutoff energy of the plane-wave basis was set to 1250 eV. The Monkhorst–Pack grid mesh[36)] was used for k-point sampling, and the number of mesh points was varied from model to model because the lattice parameters were restricted in the strained lattice models. Typically, the $5 \times 5 \times 3$ mesh was used to sample the Brillouin zone of the conventional WZ-type AlN lattice. In SCF calculations, the ensemble density functional theory[37)] was employed instead of the conventional density mixing scheme,[38)] and a considerable number of empty bands were included to

ensure convergence. The convergence tolerance for electronic energy minimization was set to 5.0×10^{-7} eV/atom. The lattice parameters and atomic positions were optimized with some constraints, namely, $a_0 = b_0$, $\alpha = \beta = 90°$, and $\gamma = 120°$, in order to maintain a hexagonal unit cell. The two-point steepest descent algorithm[39] was employed for efficient convergence under these structural constraints.

The following steps were used to study the polarization reversal in WZ-type AlN by DFT calculations. First, the relaxation of the WZ phase under axial stress and external pressure along the c-axis of the WZ-type unit cell (P_{33}) was carried out. Here, the a_0 and c_0 lattice parameters and atomic positions were fully relaxed under the assumed pressure to minimize the total energy under the given pressure conditions, and the enthalpy of the relaxed lattice was calculated. This step was performed to evaluate possible lattice deformations, such as the deformation due to the lattice mismatch between AlN thin films and substrate materials in some heteroepitaxial systems. Second, the enthalpy in the virtual NP phase was calculated. The NP phase is likely to be a transition state for the polarization reversal of the WZ phase; hence, the enthalpy difference between the transition state NP phase and original WZ phase was considered to be the activation energy of polarization reversal. Here, it was assumed that the a-axis length remained unchanged during polarization reversal and the NP phase belonged to the $P6_3/mmc$ space group. Hence, only the c-axis length of the NP phase was optimized to calculate the enthalpy, because the Al and N fractional atomic positions were fixed under the symmetry constraints of the $P6_3/mmc$ space group. The a_0 of the virtual NP phase was varied by considering the values of the strained WZ phase shown in **Fig. 2**. The NP phase with the same lattice parameters as the strained WZ phase shown in Fig. 2 was also used to elucidate the effect of the deformation on the enthalpy. Both a_0 and c_0 were relaxed only when the structure of the unstressed NP phase was optimized. Based on the results of the above two steps, the activation energy of polarization reversal was determined and correlated with E_c. For all structural relaxation calculations, the structural optimization convergence tolerance values were set as follows: electron energy of 5.0×10^{-6} eV/atom, force of 0.1 eV/nm, and atomic displacement of 5.0×10^{-5} nm. The convergence tolerance for stress was set to 0.02 GPa for the relaxation of the lattice parameters, but was not applied for the calculations on the NP phase, where a_0 and c_0 were the same as those of the WZ phase.

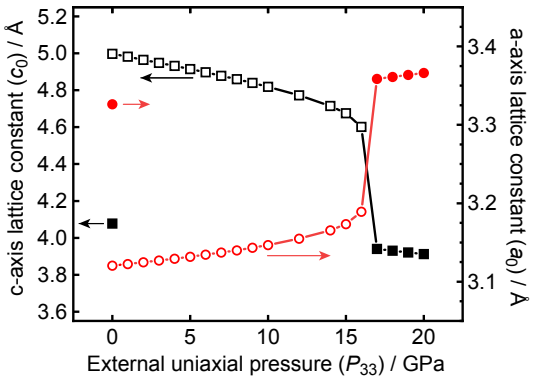

Fig. 2. Structural parameters of AlN crystallized in a WZ-type structure, $P6_3mc$, or a NP structure, $P6_3/mmc$, under a uniaxial pressure along the c-axis. The open and closed symbols indicate the resultant structure with polar and NP structures, respectively.

3. Results and discussion

Figure 2 shows the calculated lattice constants of AlN as a function of P_{33}. Here, a_0, c_0, and all atomic positions were relaxed to determine the most stable structure under uniaxial stress. Because no external pressure is applied along the a and b axes ($P_{11} = 0$ and $P_{22} = 0$), the lattice parameter a_0 increases while c_0 decreases with increasing external pressure. Moreover, a_0 and c_0 showed a jump between $P_{33} = 16$ and 17 GPa due to the transition in the lattice symmetry between the WZ phase at the lower P_{33} and NP phase at the higher P_{33}. The c-axis fractional atomic positions of N are the same as those of Al for $P_{33} = 17$ GPa, but are different for $P_{33} = 16$ GPa. These results indicate that the WZ/NP phase transition occurs between $P_{33} = 16$ and 17 GPa under the present simulation conditions. The lattice parameters of the unstressed NP phase at $P_{33} = 0$ ($a_0 = 3.326$ Å and $c_0 = 4.078$ Å) were also determined. If the in-plane lattice mismatch between the NP and WZ phases is defined as the difference in the calculated a_0 parameters between the unstrained NP phase ($a_0 = 3.326$ Å) and WZ phase ($a_0 = 3.1208$ Å), a lattice mismatch of 6.5 % is obtained. It is quite large and is indicative of the presence of a larger mismatch in the material during polarization reversal: the presence of the intermediate state, such as nucleation of the relaxed NP phase in relaxed WZ-lattice, may result in the degradation of the material because of the very large lattice mismatch. Therefore, we discuss the possible lattice deformation involving WZ and NP structures to reduce E_c for polarization reversal.

The results presented in Fig. 2 are useful for consideration of the compatibility between experimental and theoretical investigations. Experimental application of a uniaxial external pressure to the WZ phase along the c-axis in order to reproduce the calculated results is in progress in the authors' group. On the other hand, the calculated total energy and enthalpy of the NP phase must be carefully considered, because charge neutrality is established in every single [AlN] layer in the NP phase, which is similar to the case of hexagonal boron nitride (h-BN). As discussed in the literature,[40] the structural stability in h-BN cannot be investigated by conventional DFT calculations since the van der Waals interaction needs to be considered through the inclusion of the dispersion correction in the DFT functional in order to determine the physical properties of h-BN by electronic structure calculations. Therefore, the current results in Fig. 2 indicate a general trend in the stability of WZ and NP phases, but further detailed calculations must be performed, including the dispersion correction. At this stage, we only discuss some qualitative trends given by the conventional DFT calculations that

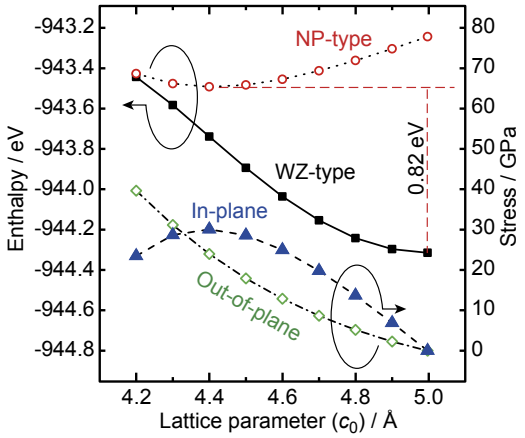

Fig. 3. Structural parameters of AlN crystallized in a WZ-type structure, $P6_3mc$, or a NP structure, $P6_3/mmc$, when the a-axis length is fixed at 3.1208 Å. The left axis shows the enthalpy in the crystal, and the right axis shows the stress in the calculated WZ-type lattice.

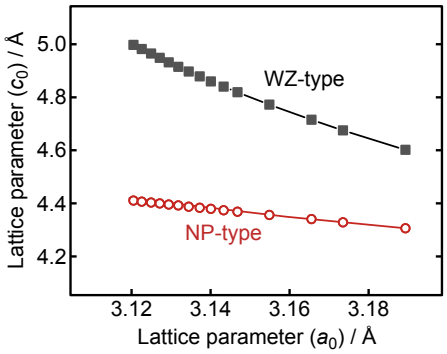

Fig. 4. Calculated c-axis length of AlN crystallized in a non-polar structure type (NP type) in the $P6_3/mmc$ symmetry as a function of the a-axis length. The lattice parameters of the WZ-type structure under axial stress in Fig. 2 are plotted again as a reference.

allow us to understand the ferroelectric properties of WZ-type phases.

Figure 3 shows the lattice deformation behavior when a_0 was fixed at 3.1208 Å (unstressed WZ-type AlN) and c_0 was varied. The unstressed c_0 was calculated to be 4.9969 Å, and the shrinkage of c_0 was considered. The calculated enthalpy of WZ-type AlN increased monotonically with decreasing c_0 due to elastic compression. By contrast, the calculated enthalpy of the NP phase had a minimum value when c_0 was 4.40 Å. Furthermore, the enthalpies of the NP and WZ phases were approximately the same for a c_0 of 4.20 Å. For polarization reversal of the WZ-type phase, the difference between the enthalpies of the unstrained WZ phase and NP phase for $c_0 = 4.40$ Å corresponds to the activation energy. Our calculated value of the activation energy (0.82 eV) is quite close to the previously reported results obtained when a_0 was fixed at the value calculated for the unstrained WZ phase during polarization reversal.[27)]

The results shown in Fig. 3 imply that polarization is reversed in the WZ phase with the assumed lattice parameters ($a_0 = 3.1208$ Å and $c_0 = 4.9969$ Å) through the NP phase with the same a_0 ($a_0 = 3.1208$ Å and $c_0 = 4.40$ Å) as that of the transition state. Based on these calculated results and assumed polarization reversal mechanism, a change in the film thickness is expected during the polarization reversal motion under an external electric field, and the estimated thickness change is approximately 12 %. Considering the experimental resolution of the available characterization tools, such as optical interferometers and X-ray diffractometers, this model should be verified by high-speed measurements.

Figure 3 also shows the stress appearing in the WZ phase under the assumed lattice parameters values. It is interesting to note that the WZ-type phase ($a_0 = 3.1208$ Å and $c_0 = 4.30$ Å) emerges under isostatic pressure conditions at approximately 30 GPa, as the values of the in-plane and out-of-plane stresses were nearly the same. Furthermore, when an external isostatic pressure of 30 GPa is applied to the WZ phase, the activation energy for polarization reversal is reduced to approximately 0.1 eV. This is almost one order of magnitude lower than the activation energy for the unstressed WZ phase. It is challenging to apply an electric field to a film maintained under an isostatic pressure of 30 GPa. However, according to our model, a polarity change is highly likely to occur under these conditions.

Next, the variation in the c_0 of the NP phase with different a_0 was considered, as summarized in **Fig. 4**. Here, the a_0 of the NP phase was varied within an assumed range, and c_0 was relaxed by DFT calculations to minimize the total energy. These calculations were performed to obtain insights into ferroelectricity in heteroepitaxial structures, where a_0 is strongly constrained due to lattice mismatch. The lattice parameters of the WZ phase shown in Fig. 2 are plotted again in Fig. 4 for reference. The relaxed c_0 of the NP phase is much smaller than that of the WZ phase with the same a_0 because of planar atomic coordination. In Fig. 4, the c_0 of the NP phase decreases with increasing a_0. As discussed for the results presented in Fig. 3, the proposed polarization reversal motion illustrated in Fig. 1 may reduce the film thickness under the transition state. The magnitude of the thickness reduction during polarization reversal motion appears to be smaller in the film with a relatively large a_0.

Figure 5(a) shows the enthalpy of the WZ and NP phases, with the lattice parameters shown in Fig. 4. With increasing a_0, the enthalpy of the WZ phase increases because of the deformation caused by a reduced c_0. The total energy values of the WZ phase with these assumed lattice parameters are provided in the supporting information (Fig. S1), and show that the WZ phase with $a_0 = 3.1208$ Å and $c_0 = 4.9969$ Å is the equilibrium structure. On the other hand, the enthalpy of the NP phase decreases with increasing a_0 and decreasing c_0. Interestingly, the enthalpy of the WZ phase exceeds that of the NP phase when a_0 exceeds 3.14 Å. This implies that AlN will crystallize in the NP form when grown heteroepitaxially

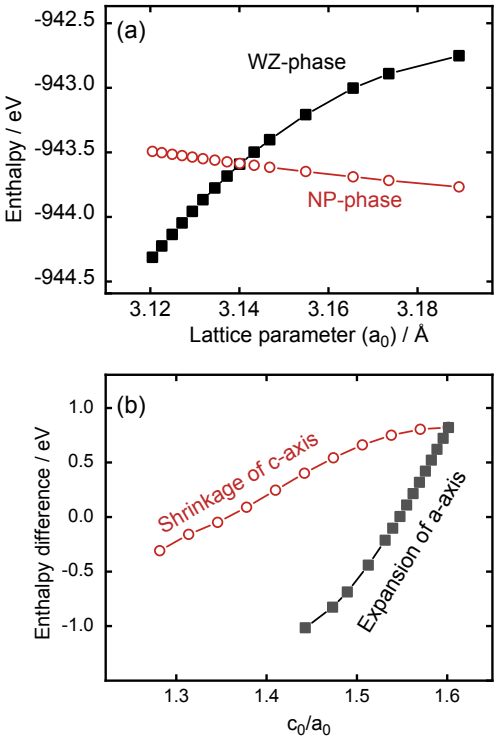

Fig. 5. (a) Enthalpy in AlN crystallized in WZ and NP types as a function of the assumed a-axis length, and (b) difference in enthalpy between WZ-type and NP-type AlN as a function of the lattice parameter ratio of c_0/a_0.

on a certain substrate, to restrict its in-plane lattice parameter to greater than 3.14 Å. However, crystallization of the NP phase may not be experimentally observed because of the extremely high internal stress, as discussed below. We must also discuss the difference between the calculated results shown in Figs. 2 and 5(a). The results shown in Fig. 2 indicate that a WZ/NP transition occurs when $a_0 \approx 3.19$ Å, while Fig. 5(a) indicates that the transition occurs at $a_0 \approx 3.14$ Å. This inconsistency arises from the difference in the constraints applied for the calculation of the NP phase and therefore, is acceptable.

The results of the enthalpy calculation shown in Fig. 2 indicate a decrease in c_0 for a fixed a_0. The results in Fig. 5(a), where a_0 is expanded, are compared to the results presented in Fig. 5(b). Here, we assume that a_0 remains unchanged during polarization reversal, implying that E_c should be correlated with the enthalpy difference between the NP and WZ phases with the same a_0. The enthalpy difference shown in Fig. 5(b) was evaluated under this assumption and plotted versus the c_0/a_0 ratio of the assumed WZ phase. The plot indicates that the decrease in the c_0/a_0 ratio results in a reduction of the enthalpy difference. In particular, when the c_0/a_0 ratio decreases, the expansion of a_0 leads to a steep decrease in the enthalpy difference.

Finally, the residual stress was studied in the NP phase to consider whether the NP/WZ transition is realistic. **Figure 6** shows the calculated stress as a function of a_0, where two major constraints (symmetry of the $P6_3/mmc$ space group and a fixed a_0) were applied. Converged results were obtained with a very high residual stress. As shown in Fig. 6, a compressive stress is generated to limit a_0, while a tensile stress emerges to maintain the expanded c_0; the magnitude of both stresses exceeds 10 GPa. According to the literature,[41),42)] the tensile and compressive strengths of AlN are approximately 0.1 and 1 GPa, respectively, suggesting that the AlN film in Fig. 6 is subject to a very high residual stress. In experiments, AlN thin films often break due to dielectric breakdown under the bias of a high electric field strength. The mechanism for the breakdown behavior is currently unclear. The calculation results shown in Fig. 6 suggest that the very high stress during the NP/WZ transformation may be an origin of the observed breakdown behavior. When polarization reversal is triggered under a high electric field, the film is damaged due to the high stress in the transient NP phase.

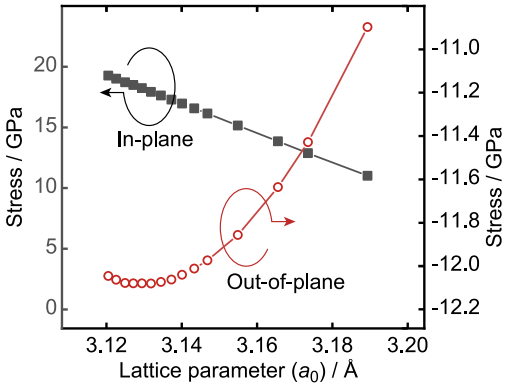

Fig. 6. Calculated stress in the NP phase as a function of the a-axis length.

4. Conclusions

The ferroelectric behaviors of WZ-type compounds were investigated by DFT calculations. It was confirmed that the shrinkage of c_0 and expansion of a_0 are favorable for reducing E_c, based on the assumption that the NP phase with symmetries of the $P6_3/mmc$ space group appeared as a transition state during polarization reversal. The activation energy for polarization reversal was 0.8 eV, which is similar to the value obtained in previous studies.[27)] Nevertheless, the lattice strain for decreasing c_0 and increasing a_0 appears to be sufficient to lower E_c. In addition, the residual stress in the NP phase during polarization reversal was found to be as high as 30 GPa. This study indicates that such a high residual stress may be essential for the development of electronic and ferroelectric WZ-type compounds.

Conflict of interests The authors declare that there is no conflict of interest.

Part of this study was performed at the Tokodai Institute for Elemental Strategy (TIES), supported by the grant number JPMXP0112101001. This work was partly supported by the JST and PRESTO under grant number JPMJPR20B3.

References

1) D. Jena, R. Page, J. Casamento, P. Dang, J. Singhal, Z. Zhang, J. Wright, G. Khalsa, Y. Cho and H. G. Xing, *Jpn. J. Appl. Phys.*, 58, SC0801 (2019).
2) I. Abid, R. Kabouche, C. Bougerol, J. Pernot, C. Masante, R. Comyn, Y. Cordier and F. Medjdoub, *Micromachines-Basel*, 10, 690 (2019).
3) B. Chen, F. Chu, X. Liu, Y. Li, J. Rong and H. Jiang, *Appl. Phys. Lett.*, 103, 031118 (2013).
4) M. Akiyama, T. Kamohara, K. Kano, A. Teshigahara, Y. Takeuchi and N. Kawahara, *Adv. Mater.*, 21, 593–596 (2009).
5) Y. Song, C. Perez, G. Esteves, J. S. Lundh, C. B. Saltonstall, T. E. Beechem, J. I. Yang, K. Ferri, J. E. Brown, Z. Tang, J. P. Maria, D. W. Snyder, R. H. Olsson, III, B. A. Griffin, S. E. Trolier-McKinstry, B. M. Foley and S. Choi, *ACS Appl. Mater. Inter.*, 13, 19031–19041 (2021).
6) T. Ohsawa, S. Ueda, M. Suzuki, Y. Tateyama, J. R. Williams and N. Ohashi, *Appl. Phys. Lett.*, 107, 171604 (2015).
7) K. Furuta, K. Hirata, S. A. Anggraini, M. Akiyama, M. Uehara and H. Yamada, *J. Appl. Phys.*, 130, 024104 (2021).
8) S. Manna, G. L. Brennecka, V. Stevanović and C. V. Ciobanu, *J. Appl. Phys.*, 122, 105101 (2017).
9) M. Uehara, Y. Amano, S. A. Anggraini, K. Hirata, H. Yamada and M. Akiyama, *Ceram. Int.*, 47, 16029–16036 (2021).
10) S. Manna, K. R. Talley, P. Gorai, J. Mangum, A. Zakutayev, G. L. Brennecka, V. Stevanović and C. V. Ciobanu, *Phys. Rev. Appl.*, 9, 034026 (2018).
11) H. Liu, F. Zeng, G. Tang and F. Pan, *Appl. Surf. Sci.*, 270, 225–230 (2013).
12) X. Hu, Z. Tai and C. Yang, *Mater. Lett.*, 217, 281–283 (2018).
13) T. Yokoyama, Y. Iwazaki, Y. Onda, T. Nishihara, Y. Sasajima and M. Ueda, *IEEE Trans. Ultrason., Ferroelectr, Freq. Control*, 61, 1322–1328 (2014).
14) T. Yokoyama, Y. Iwazaki, T. Nishihara and J. Tsutsumi, *Proc. 2016 IEEE International Ultrasonics Symposium (IUS)*, Sept. 18–21, Tours, France, (2016) pp. 1–4.
15) M. Uehara, H. Shigemoto, Y. Fujio, T. Nagase, Y. Aida, K. Umeda and M. Akiyama, *Appl. Phys. Lett.*, 111, 112901 (2017).
16) M. Uehara, T. Mizuno, Y. Aida, H. Yamada, K. Umeda and M. Akiyama, *Appl. Phys. Lett.*, 114, 012902 (2019).
17) S. Fichtner, N. Wolff, F. Lofink, L. Kienle and B. Wagner, *J. Appl. Phys.*, 125, 114103 (2019).
18) J. Hayden, M. D. Hossain, Y. Xiong, K. Ferri, W. Zhu, M. V. Imperatore, N. Giebink, S. Trolier-McKinstry, I. Dabo and J. P. Maria, *Phys. Rev. Mater.*, 5, 044412 (2021).
19) W. Zhu, J. Hayden, F. He, J. I. Yang, P. Tipsawat, M. D. Hossain, J. P. Maria and S. Trolier-McKinstry, *Appl. Phys. Lett.*, 119, 062901 (2021).
20) K. Ferri, S. Bachu, W. Zhu, M. Imperatore, J. Hayden, N. Alem, N. Giebink, S. Trolier-McKinstry and J. P. Maria, *J. Appl. Phys.*, 130, 044101 (2021).
21) M. Uehara, R. Mizutani, S. Yasuoka, T. Shiraishi, T. Shimizu, H. Yamada, M. Akiyama and H. Funakubo, *Appl. Phys. Lett.*, 119, 172901 (2021).
22) D. Wang, P. Wang, B. Wang and Z. Mi, *Appl. Phys. Lett.*, 119, 111902 (2021).
23) S. Yasuoka, T. Shimizu, A. Tateyama, M. Uehara, H. Yamada, M. Akiyama, Y. Hiranaga, Y. Cho and H. Funakubo, *J. Appl. Phys.*, 128, 114103 (2020).
24) R. Deng, S. R. Evans and D. Gall, *Appl. Phys. Lett.*, 102, 112103 (2013).
25) H. Moriwake, A. Konishi, T. Ogawa, K. Fujimura, C. A. J. Fisher, A. Kuwabara, T. Shimizu, S. Yasui and M. Itoh, *Appl. Phys. Lett.*, 104, 242909 (2014).
26) A. Konishi, T. Ogawa, C. A. J. Fisher, A. Kuwabara, T. Shimizu, S. Yasui, M. Itoh and H. Moriwake, *Appl. Phys. Lett.*, 109, 10.2903 (2016).
27) H. Moriwake, R. Yokoi, A. Taguchi, T. Ogawa, C. A. J. Fisher, A. Kuwabara, Y. Sato, T. Shimizu, Y. Hamasaki, H. Takashima and M. Itoh, *APL Mater.*, 8, 121102 (2020).
28) A. Krishnamoorthy, S. C. Tiwari, A. Nakano, R. K. Kalia and P. Vashishta, *Nanotechnology*, 32, 49LT02 (2021).
29) K. Furuta, K. Hirata, S. A. Anggraini, M. Akiyama, M. Uehara and H. Yamada, *J. Appl. Phys.*, 130, 024104 (2021).
30) S. Clima, C. Pashartis, J. Bizindavyi, S. R. C. McMitchell, M. Houssa, J. V. Van Houdt and G. Pourtois, *Appl. Phys. Lett.*, 119, 172905 (2021).
31) M. Noor-A-Alam, O. Z. Olszewski and M. Nolan, *ACS Appl. Mater. Inter.*, 11, 20482–20490 (2019).
32) K. Yazawa, D. Drury, A. Zakutayev and G. L. Brennecka, *Appl. Phys. Lett.*, 118, 162903 (2021).
33) B. Riah, J. Camus, A. Ayad, M. Rammal, R. Zernadji, N. Rouag and M. A. Djouadi, *Coatings*, 11, 1063 (2021).
34) S. J. Clark, M. D. Segall, C. J. Pickard, P. J. Hasnip, M. J. Probert, K. Refson and M. C. Payne, *Z. Kristallogr.*, 220, 567–570 (2005).
35) J. P. Perdew, A. Ruzsinszky, G. I. Csonka, O. A. Vydrov, G. E. Scuseria, L. A. Constantin, X. Zhou and K. Burke, *Phys. Rev. Lett.*, 100, 136406 (2008).
36) H. J. Monkhorst and J. D. Pack, *Phys. Rev. B*, 13, 5188–5192 (1976).
37) M. C. Payne, M. P. Teter, D. C. Allan, T. A. Arias and J. D. Joannopoulos, *Rev. Mod. Phys.*, 64, 1045–1097 (1992).
38) P. Pulay, *Chem. Phys. Lett.*, 73, 393–398 (1980).
39) J. Barzilai and J. M. Borwein, *IMA J. Numer. Anal.*, 8, 141–148 (1988).
40) T. Gruber and A. Grüneis, *Phys. Rev. B*, 98, 134108 (2018).
41) W. Chen and G. Ravichandran, *J. Am. Ceram. Soc.*, 79, 579–584 (1996).
42) D. G. Zong, C. W. Ong, M. Aravind, M. P. Tsang, C. L. Choy, D. Lu and D. Ma, *Philos. Mag.*, 84, 3353–3373 (2004).